



HAL
open science

A 3D atlas of the human developing pancreas to explore progenitor proliferation and differentiation.

Adrian Villalba, Yorick Gitton, Megumi Inoue, Virginie Aiello, Raphaël Blain, Maryne Toupin, Séverine Mazaud-Guittot, Latif Rachdi, Henrik Semb, Alain Chédotal, et al.

► To cite this version:

Adrian Villalba, Yorick Gitton, Megumi Inoue, Virginie Aiello, Raphaël Blain, et al.. A 3D atlas of the human developing pancreas to explore progenitor proliferation and differentiation.. 2023. hal-04302461

HAL Id: hal-04302461

<https://cnrs.hal.science/hal-04302461v1>

Preprint submitted on 27 Nov 2023

HAL is a multi-disciplinary open access archive for the deposit and dissemination of scientific research documents, whether they are published or not. The documents may come from teaching and research institutions in France or abroad, or from public or private research centers.

L'archive ouverte pluridisciplinaire **HAL**, est destinée au dépôt et à la diffusion de documents scientifiques de niveau recherche, publiés ou non, émanant des établissements d'enseignement et de recherche français ou étrangers, des laboratoires publics ou privés.

Title: A 3D atlas of the human developing pancreas to explore progenitor proliferation and differentiation.

Running title: A 3D map of the human fetal pancreas.

Adrian Villalba^{1,+}, Yorick Gitton^{2,+}, Megumi Inoue², Virginie Aiello¹, Raphaël Blain², Maryne Toupin³, Séverine Mazaud-Guittot³, Latif Rachdi¹, Henrik Semb⁴, Alain Chédotal^{2,*} and Raphaël Scharfmann^{1,*,#}.

¹ Université Paris Cité, Institut Cochin, CNRS, INSERM, Paris, France.

² Sorbonne Université, INSERM, CNRS, Institut de la Vision, Paris, France.

³ Univ Rennes, IRSET (Institut de Recherche en Santé, Environnement et Travail), INSERM, EHESP, UMR_S 1085, Rennes, France.

⁴ Institute of Translational Stem Cell Research, Helmholtz Diabetes Center, Helmholtz Zentrum München, München, Germany.

+ These authors contributed equally.

* Co-corresponding authors.

Lead contact: raphael.scharfmann@inserm.fr

Word count: 4565

Abstract

The pancreas is a critical endocrine and exocrine dual gland. While pancreas organoid models have been extensively explored for medical applications ranging from metabolic to oncologic conditions, there are still gaps in our understanding of the normal developmental trajectories of pancreatic cells during *in vivo* human ontogenesis. Here we mapped their spatial and chronological dynamics using 3D imaging of cleared human embryonic and fetal pancreases. Unexpectedly, we detected insulin immune-positive cells as soon as 5 post-conceptual weeks, two weeks earlier than previously observed. We identified a central niche as the onset of the earliest insulin cells production, and detected extra-pancreatic loci within the adjacent developing gut. Conversely, proliferating pancreatic progenitors were located in the periphery of the epithelium, suggesting the existence of two separated pancreatic niches for differentiation and proliferation. We next validated an explant culture system enabling *in vitro* proliferation of pancreatic progenitors. This unveiled a mitogenic effect of PDGFAA in progenitors acting through the pancreatic mesenchyme. Overall, this work presents a first 3D atlas of the human developing pancreas charting both endocrine and proliferating cells across early development.

Keywords

Human Fetal Pancreas; Light Sheet Fluorescence Microscopy; Pancreatic Progenitors; Proliferating Cells, Insulin-producing Cells, PDGF signaling.

Introduction

The pancreas is a vital organ involved in multiple crucial functions from glucose homeostasis to digestion¹. It is a mixed gland composed of an exocrine and an endocrine fraction. The exocrine part contains acinar cells releasing enzymes like Carboxypeptidase A1 (CPA1) and Amylase (AMY) through a ductal network draining into the duodenum. The endocrine fraction, clustered in the islets of Langerhans, accounts for 1% of the pancreatic mass. Pancreas dysfunction is associated with a large spectrum of interconnected disorders, including diabetes mellitus, pancreatitis, and pancreatic cancer, which are major health burdens worldwide². During embryonic development, the pancreas originates from the foregut endoderm and undergoes morphogenesis, characterized by extensive proliferation, migration, and differentiation of distinct cell populations³. Among them, the endocrine cells, which produce hormones such as insulin (beta cells), glucagon (alpha cells), and somatostatin (delta cells), are derived from a subset of pancreatic progenitor cells that undergo endocrine differentiation¹. Understanding the regulation of this process is subject of intense research, bearing significant implications for developmental biology and regenerative medicine⁴⁻⁶.

Rodent pancreas development has been studied in great details during the past decades through the use, among other technologies, of genetically modified mouse models^{7,8}. However, the developmental and cellular mechanisms underlying the formation and maturation of the human pancreas are far less understood. The development of the human pancreas begins during the fourth post-conceptual week (PCW4), when dorsal and ventral pancreatic buds emerge from the endodermal cells of the developing gut tube^{1,9,10}. These epithelial buds contain pancreatic progenitors that express key transcription factors such as PDX1, SOX9, NKX6-1, FOXA2 and PTF1A^{11,12}. They develop in an intricate fashion within the surrounding mesodermal-derived mesenchyme and undergo fusion, branching morphogenesis, differentiation of endocrine and exocrine cells, and establishment of functional connections with the surrounding organs¹⁰. Pancreatic progenitor cell differentiation into endocrine cells is tightly regulated by various transcription factors and signaling pathways¹³. Furthermore, the proliferation of pancreatic progenitor cells is a critical aspect of pancreas development and the balance between proliferation and differentiation is essential for the proper development of the

organ. In this context, the way the human embryonic and fetal pancreas develops represents a critical source of information^{10,14,15}.

Recently, the combination of light-sheet fluorescent microscopy (LSFM) and tissue clearing has enabled the three-dimensional (3D) visualization of cellular and tissue architecture in unprecedented detail and resolution^{16,17}. Moreover, the integration of imaging data across different developmental stages has led to the creation of tissue atlases, which provide comprehensive cellular maps of specific tissues or organs^{18–20}. These cell atlases are invaluable resources for understanding the heterogeneity and complexity of human biology.

So far, 2D descriptions with a limited number of markers did not capture the topographic relationship between pancreatic progenitors and endocrine cell types. In this study, we leveraged our expertise in LSFM and tissue clearing^{17,21} to revisit the early stages of human pancreas development (PCW5-11), which retain their topographic integrity. We specifically aimed at investigating the spatiotemporal dynamics of INS⁺ cell differentiation and progenitor proliferation in the developing human pancreas using LSFM to build a human developing pancreas atlas. Our results reveal novel insights into the cellular mechanisms underlying pancreatic development and provide a foundation for future studies aimed at gaining further insights into human pancreas development.

Results

Human embryonic and fetal pancreases display isometric growth from 5 to 11 PCW

Significant progress in conventional 2D immunostainings provided highly valuable information about human pancreas development¹¹. However, there is limited work providing 3D analyses of the human embryonic or fetal pancreas. Here, we report for the first time the use of iDISCO+²² tissue clearing and LSM to track the morphological development of the human embryonic and fetal pancreas. Conventional immunostainings indicated that pancreatic progenitors are immunoreactive for the transcription factors SOX9, PDX1 and NKX6.1^{10,23}. We performed triple staining that demonstrated similar pancreatic expression patterns for all 3 markers in both conventional immunostaining (Supplementary Fig. 1a) and 3D imaging (Supplementary Fig. 1b and Movie 1). Therefore, during this developmental period PCW5-11), these 3 markers (SOX9, PDX1 and NKX6.1) can be interchangeably used to identify progenitors. SOX9 staining, in an intact transparent PCW7 human embryo, allowed to precisely visualize the pancreas in the upper left abdomen, highlighted in white (Fig. 1a, b, and Movie 2). We next immunolabelled for SOX9 PCW5-11 pancreas, followed by clearing and LSM. In the mouse, the pancreas develops from two independent buds that will fuse later on^{24,25}. However, the timing of this process was poorly documented in human. At PCW5, both ventral and dorsal buds were detected (Fig. 1c, and Movie 3), whereas at PCW6 they had fused and formed complete a single pancreatic primordium (Fig. 1d).

3D imaging in our PCW5-11 developmental series revealed an obvious increase in pancreatic size (Fig. 1e). To quantify human pancreas growth, we measured their lengths along the longitudinal axis and diameters across the dorso-ventral axis. Both length and diameter increased across development from PCW5-11 (n= 29 pancreases) (Fig. 1f, g). The growth in both length and diameter showed a 6-fold increase from PCW5 to PCW11, revealing a positive linear correlation between pancreatic size and age. The quantification of the diameter to length ratio showed that it remained stable (Fig. 1h), indicating that pancreas growth is homothetic during the first trimester of gestation.

INS⁺ cells arise around 5 PCW and are located in the center of the human developing pancreas

3D imaging allows the precise spatial location of specific pancreatic cell populations. We next asked when and where do the first INS^+ cells appear. Previous reports on human fetal pancreases based on 2D immunohistochemistry detected the earliest INS^+ cells around PCW7^{11,26}. Here, we were able to detect the presence of INS^+ clusters as early as PCW5.7 (Fig. 2a). At this early stage, they were restricted to the dorsal bud and absent from the ventral bud (Fig. 2a, and Movie 4), indicating that, as in the mouse²⁷, INS^+ cells first appear in the dorsal pancreas in human. Recent studies by conventional 2D immunostaining revealed the existence of INS^+ cells in the human fetal gut between PCW10-19²⁸. We could detect extra-pancreatic INS^+ clusters far earlier between PCW6.3 and PCW10.6, in the fetal gut and also at the junction between the gut and the pancreas (Fig. 2b-e, and Movie 5).

We next quantified the number of pancreatic INS^+ clusters on 19 samples between PCW5.4 and PCW11. We observed few INS^+ clusters from PCW5.4 to 7.5 (9.25 ± 5.65 , mean \pm SD, n=8), with a sharp increase at later stages ($4,307 \pm 152.34$, mean \pm SD, n=3 at PCW11) (Fig. 2f, g). We also manually quantified using conventional immunostaining, the number of INS^+ cells per cluster in paraffin sections from 3 pancreases (180-240 sections per specimen) at PCW6. We found that the first INS^+ clusters contain between 1 to 5 INS^+ cells (Fig. 2h).

We next analyzed the location of these INS^+ clusters and observed their preferential location in the center of the pancreas, being almost absent from the periphery. INS^+ clusters were aligned along the longitudinal axis of the pancreas, (Fig. 2i, j, and Movie 6). We mapped in 3D the distribution of INS^+ clusters to the centroid of the $SOX9^+$ pancreatic epithelium in z-slices from 3D scans from 3 pancreases at PCW9. In all 3 pancreases, the vast majority of the INS^+ clusters were located closer to the center rather than to the periphery (Fig. 2k).

Our data thus strongly suggest the existence of a niche in the center of the pancreas promoting the differentiation of progenitors towards an INS^+ cell fate. Given that vascularization has been suggested as an important player in beta cell development in mice²⁹, we mapped vascular markers with regards to INS^+ cells in the human embryonic/fetal pancreas. The general marker for mature vascular endothelial cells CD34 was expressed in a uniform network of vessels intermingled with $SOX9^+$ pancreatic progenitors, without obvious differential distribution from center to peripheral domains

(Supplementary Fig. 2a). Noticeably, the whole extent of the developing pancreas was devoid of the more specific arterial marker SMA at PCW9 (Supplementary Fig. 2b).

Finally, we compared pancreatic development between human and mice by LSFM (Fig. 3a, c). As expected, pancreatic length and diameter increased in mouse embryos between E12 and E16 (Fig. 3d, e). However, the diameter/length ratio increased across development (Fig. 3f), which is different from what we observed in human pancreatic samples from PCW5-11. Likewise, the number of INS^+ clusters increased in mice from E10 to E16 (Fig. 3g, h).

Proliferating pancreatic progenitors are restricted to the periphery of the epithelium

Next, we sought to correlate human pancreatic differentiation dynamics with proliferation kinetics across the first trimester. KI67/PDX1 double staining indicated that 20 to 30% (n=3) of pancreatic progenitors ($PDX1^+$) are proliferating from PCW7-11 (Fig. 4a, b) while differentiated INS^+ cells proliferate at a far lower rate at a ratio around 1% from PCW 9-11 (n=3) (Fig. 4c, d).

By selecting cell surface markers and using FACS, we had previously subdivided human fetal pancreatic progenitors into a number of populations with $ECAD^+CD142^+SUSD2^-$ (pink) giving rise to $ECAD^+CD142^-SUSD2^-$ (green) and finally to $ECAD^{low}CD142^-SUSD2^+$ (blue)^{30,31}. Here, we first reanalyzed our transcriptomic datasets³¹, asking whether proliferation markers change from one progenitor population to the other. By using our previously validated list of pancreatic proliferation markers³², we observed a downregulation from population A to C, including canonical proliferation genes such as *KI67*, *PCNA* and *CDK1* (Fig. 4e). This indicates that progenitors proliferate at different rates in the human embryonic/fetal pancreas and proliferation decreases along with endocrine differentiation. The next question concerned the spatial location of proliferating progenitors. We took advantage from recurrent access to fresh pancreases and used EdU—a thymidine analogue—to label cells entering S-phase. Proliferating pancreatic progenitors ($PDX1^+EdU^+$) were found to be highly enriched at the periphery of the pancreas, while their frequency in the center was extremely low (Fig. 4f). The distribution pattern of pancreatic proliferating progenitors was mathematically analyzed by computing the Ripley K function ($K(r)$)³³ in 2D images at PCW7, 9 and 11. It showed that $PDX1^+KI67^+$ progenitors are clustered together in aggregates, rather than randomly distributed (Fig. 4g, h). We finally determined whether proliferating $PDX1^+KI67^+$ cells

might represent acinar cells that express carboxypeptidase A1 (CPA1). We observed that the human fetal pancreas is enriched in CPA1⁺ cells in the periphery, rather than in the center (Fig. 4i), further supporting that the inner fetal pancreas is an endocrine niche. We also found that the majority of these CPA1⁺ cells lacked KI67 expression. Overall, our data further support the existence of a niche of proliferation for pancreatic progenitors in the periphery of the human embryonic and fetal pancreas.

PDGFAA induces the proliferation of human pancreatic progenitors in vitro

We finally searched for signaling pathways that induce the proliferation of human pancreatic progenitors. For this purpose, we cultured human fetal pancreases over a floating filter disk in a gas-liquid interface for either 3 or 7 days. Under such conditions, pancreatic progenitors were maintained up to 7 days keeping a similar proliferation ratio (16.94±7.72 and 14.54±0.78 % of PDX1⁺ cells at day 3 and 7, mean±SD, n=5-6 per group) than in vivo (19.98±2.42, mean±SD, n=3 at PCW9) (Supplementary Fig. 3a). Furthermore, the progenitors kept their multipotent phenotype during the full culture period, as assessed by the expression of PDX1 and NKX6.1 (Supplementary Fig. 3b). Gain- and loss-of-function experiments using either FGF10³⁴ or the MEK1 inhibitor PD98059³⁵, respectively, did not alter the PDX1⁺KI67⁺ ratio (data not shown). We next switched to a culture medium that contains ALK5i, noggin and nicotinamide that showed a reduction in the PDX1⁺/KI67⁺ ratio to around 5% to be used to search for factors that enhance progenitor proliferation. Our previous transcriptomic data³⁰ indicated that PDGFRA and PDGFRB are specifically expressed by human fetal pancreatic mesenchyme but not in pancreatic epithelial cells (Fig. 5a) and we further confirmed such data by immunostaining (Fig. 5b, c). We thus treated pancreatic explants with PDGFAA for 7 days. The macroscopic architecture of the explants remained unaffected (Fig. 5d). We observed a three-fold increase in the number of proliferating progenitors (PDX1⁺KI67⁺) (Fig. 5e). We also observed changes in the microscopic tissue architecture following PDGFAA treatment. While the lumen size increased in control explants during the culture period, upon PDGFAA treatment, their size became more similar to that observed in vivo (Fig. 5f, g). Overall, through the establishment of a culture model of human fetal pancreases, we suggested that PDGF acts indirectly through mesenchymal cells to induce progenitor cell proliferation.

Discussion

There is an urgent need to improve the development of stem cell-derived human beta cells, to build novel therapies for the treatment of type 1 diabetes³⁶. Most of the current protocols attempt to recapitulate beta cell neogenesis processes^{5,37-39}. However, the vast majority of our knowledge on beta cell differentiation comes from studies on mouse pancreas development^{3,40} along with a limited human development comparisons. Nevertheless, some significant differences have also been observed. For example, human and mouse islets differ in terms of dynamics of endocrinogenesis⁴²⁻⁴⁴, shape⁴⁵, gene expression⁴⁶⁻⁴⁸, glucose transport and insulin secretion^{49,50}. However, a detailed timeline and topographic description of human embryonic and fetal pancreatic cell proliferation and differentiation remained to be established. Here, through the INSERM-funded *HUMAN DEVELOPMENTAL CELL ATLAS* consortium (<https://hudeca.genouest.org/>), we could access a large collection of fresh pancreases between PCW5 and PCW11 allowing more than 20 replicates in some experiments and thus deep analyses and quantifications of human pancreatic development.

The majority of previous histological data on the developing mouse and human pancreas has been generated using conventional 2D sections^{10,11,26,51}, an approach with some limitations when searching for rare and isolated cell types⁵². Recently, a 3D description of the developing mouse pancreas was published⁵³. It provided a comprehensive view of the cellular composition and topological relationships of embryonic pancreatic cells at different stages of development, with a focus on INS⁺, GCG⁺ and endothelial cells. Here, we employed a similar pipeline to generate the first 3D atlas of the developing human pancreas by *in toto* staining, tissue clearing and LSFM imaging. We focused on the first trimester, at the time the first endocrine cells are generated¹⁰. An interesting observation is our detection of two pancreatic buds, ventral and dorsal, prior to their fusion. We also detected the first INS⁺ cells in the dorsal pancreas, similar to what has been described in mouse and zebrafish embryonic pancreases^{27,54,55}. Here we could detect INS⁺ cells at around PCW5, almost 2 weeks earlier than previously described¹¹. We also confirm the existence of extra-pancreatic INS⁺ cells in the gut region adjacent to the pancreas²⁸, but observed them much earlier than previously described. Moreover, we also found extra-pancreatic INS⁺ cells located in the duct draining the duodenum. Whether these INS⁺ cells differentiate in situ or migrate from the pancreas is still unknown, as is their function.

Our data show that the earliest INS^+ cells are either isolated or form very small clusters (of about 4-5 cells), when in adult, islets contain hundreds of INS^+ cells. Using KI67 as a surrogate for proliferation, we found that human embryonic and fetal INS^+ cells exhibit a low proliferation rate. This suggests that islet do not forms by proliferation *in situ* of preexisting INS^+ cells, consistent with our previous data using a reconstituted model of transplantation of human embryonic pancreas into immune-incompetent mice⁵⁸. Additionally, similar observations from mouse chimeras further support the polyclonal origin of pancreatic islets^{59,60}. We thus postulate that in human mature islets form by the aggregation of preexisting INS^+ cells. The mechanisms regulating such process in the human pancreas remains unknown. Mouse data suggest that endocrine cell differentiation is followed by epithelial-mesenchymal transition, migration and aggregation⁶¹. However, in an alternative hypothesis, INS^+ cells could differentiate from endocrine progenitors located within a single epithelial cord while maintaining in contact with this structure, forming a peninsula and next an islet⁶². Thus, the dynamics of human islets morphogenesis remain to be elucidated.

We raised questions regarding the earliest differentiation of INS^+ cells and their location. INS^+ cells were preferentially located in the center of the pancreas where they were tightly aligned, while almost absent in the periphery, suggesting the existence of a highly specific differentiation niche for endocrinogenesis in the inner part of the pancreas. The signals that control this specific spatial pattern of differentiation remain unknown. Although vascularization has been shown to play major roles in mouse beta cell development^{29,63,64}, we did not observe a correlation between the location of INS^+ cells and the vascular tree. Whether the specific location of the first human INS^+ cells in the human fetal pancreas is influenced by nerves, an important player in beta cell physiology⁶⁵, remains to be explored. A reduced oxygen tension in the center of the pancreas versus the periphery, could also promote central endocrinogenesis. However, we previously demonstrated that beta cell differentiation was reduced under hypoxia and increased when oxygen tension was elevated both in rat and mouse cultured fetal pancreases^{66,67}. Another hypothesis is that the intra-pancreatic mesenchyme represents a niche for endocrinogenesis. However, in rodents, the mesenchyme regulates the expansion of early pancreatic progenitors^{7,68-70}, but its depletion either *in vitro* or *in vivo* does not inhibit endocrine cell differentiation^{71,72}. In this context, we are currently testing the hypothesis that the mesenchyme located in the inner and peripheral regions of the pancreas are different.

Our KI67 data indicate that the proliferation rate of INS^+ cells is extremely limited during the second part of the first trimester of gestation, and about 20 times lower than other pancreatic progenitors. This demonstrates that the amplification pool for endocrinogenesis is at the level of pancreatic progenitors and not INS^+ cells. This is in agreement with data obtained in mouse embryos where fetal pancreatic progenitors proliferate far more efficiently than beta cells and their number is increased by signals such as FGF7 and FGF10^{35,69}. Information remains scarce on signals that increase human progenitor cell proliferation. We observed that in contrast with INS^+ cells, progenitor proliferation is restricted to the periphery of the pancreas. These findings suggest that endocrine cell differentiation and progenitor proliferation are differentially regulated processes during human pancreatic development.

Here we developed a culture system to study human progenitor cell proliferation, using a strategy previously used in rat embryos⁶⁹. Accordingly, we found that in human embryonic pancreas cultures progenitors proliferate for at least 7 days at a similar ratio than in vivo. By using this in vitro model, we demonstrate that PDGFAA, a molecule produced in the fetal pancreas by epithelial⁷⁴ and vascular smooth muscle cells⁷⁵, enhances the proliferation of pancreatic progenitors. Recently, *PDGFRA* mRNA was found to be enriched in the pancreatic mesenchyme^{74,75}, in agreement with our transcriptomic data³⁰ and with single cell transcriptomic data derived from the DESCARTES Atlas (<https://descartes.brotmanbaty.org/>). We confirmed here that the expression PDGFR is restricted to the pancreatic mesenchyme, suggesting that PDGF exerts an indirect influence on pancreatic progenitor cell proliferation by affecting mesenchymal cells.

Altogether, we present here the first attempt to build a 3D atlas of the developing human pancreas. Overall, this resource sheds light on when and where first INS^+ cells appear do, as well as pancreatic proliferating progenitors. Furthermore, we also describe the mitogenic effect of PDGFAA in the pancreatic epithelium. Our 3D imaging pipeline will allow researchers to explore the developing anatomy of the pancreas in a spatial context, and to visualize the relationships between different structures and cell types. Based on histological and transcriptomic data⁷⁶, the human embryonic and fetal pancreas contains six major cell types: epithelial, mesenchymal, endothelial, immune, neural and erythroid. Within the epithelial compartment, we have focused on the spatial location of multipotent progenitors, differentiated INS^+ cells, and acinar CPA1⁺ cells. Nevertheless, many other

differentiated cells remain to be mapped across development. This information holds great potential in enhancing our understanding of the underlying mechanisms driving embryonic and fetal pancreatic development, and potentially this knowledge could further improve the generation of stem cell derived beta cells.

Material and methods

Human and mouse embryonic and fetal pancreatic tissues

Human embryonic and fetal pancreatic tissues (5-11 post-conceptional weeks, PCW) were obtained through the INSERM Cross-Cutting Scientific Program HuDeCA from surgical abortions in accordance with the French bioethics legislation and INSERM guidelines (Ramond et al., 2017; Ramond et al., 2018). Donors written consent was obtained, along with approval from Agence de Biomédecine, the competent authority in France. Fetal ages are displayed as PCW, staged based on morphometric correction as described before⁷⁸. All specimens were initially selected based on macroscopic morphological criteria, excluding samples with obvious malformations. In cases where visual determination of sex was not possible, PCR-based chromosome screening using DNA from biopsies was performed as previously described²¹. For labelling, a minimum of 3 samples per age were employed in every experiment (Table 1 and 2), while for in vitro experiments we employed a minimum of 5 pancreases per condition.

Mouse fetal pancreases were obtained from pregnant C57BL/6J mice purchased from the Janvier Breeding Center (LeGenet, St Isle, France). Mice were killed by CO₂ asphyxiation according to French Animal Care Committee guidelines and pancreases from embryos at E10, E12 and E16 (at least 6 embryos per age) were dissected and fixed as previously described (Huijbregts et al., 2019).

Conventional 2D immunohistochemistry

Human embryonic and fetal pancreases were fixed in formalin, embedded in paraffin and sectioned (5 µm-thick) as previously described (Castaing et al., 2005; Ramond et al., 2017). The following primary antibodies were used: mouse anti-insulin (1:1,000, I2018, Sigma-Aldrich), goat anti-SOX9 (1:1,000, AF3075, R&D Systems), mouse anti-E-Cadherin (1:200, 610182, BD Biosciences), mouse anti-NKX6.1 (1:1,000, F55A12, DSHB), mouse anti-KI67 (1:100, 550609, BD Biosciences), rabbit anti-PDX1⁸² (1:1,000), rabbit anti-PDGFR α (1:500, ab124392, Abcam), rabbit anti-PDGFR β (1:500, ab32750, Abcam) and goat anti-CPA1 (1:400, AF2856, R&D Systems).

The secondary antibodies employed were: anti-rabbit Alexa Fluor 488 (1:400, A11034, Life Technologies) and Alexa Fluor 555 (1:400, ab150062, Abcam); anti-mouse Alexa Fluor 488 (1:400, ab150105, Abcam), Alexa Fluor 594 (1:400, 115 585 003, Jackson

ImmunoResearch), and Alexa Fluor 647 (ab150111); and anti-goat Alexa Fluor 488 (1:400, ab150129, Abcam). EdU revelation was performed using the Click EdU Alexa 555 imaging kit (Thermo Fisher Scientific). Nuclei were stained with Hoechst 33342 (0.3 mg/ml, Invitrogen).

We manually counted the number of INS⁺ cells per cluster in all the 5- μ m thick sections of 3 pancreases at 6 PCW (between 180 and 240 sections per specimen). The percentage of PDX1⁺/KI67⁺ (at 7, 9 and 11PCW) and INS⁺/KI67⁺ cells (at 9 and 11PCW) were quantified on 6 sections per pancreas (3 pancreases per age). The spatial distribution of PDX1⁺/KI67⁺ progenitors was performed by computing the Ripley K function (K(r)) to determine the distribution of points in a 2D space³³. To do that, the PDX1⁺/KI67⁺ progenitors were mapped with x,y coordinates in 2D images at 7, 9 and 11 PCW (a minimum of n = 20 images per developmental stage), using FIJI⁸³. Then, the Ripley K function (K(r)) was computed for every image by implementing the R library spatstat for spatial statistics as previously described⁸⁴.

3D immunostaining

Embryonic and fetal samples were fixed by immersion in formalin at 4°C for 1 to 5 days depending on size. For tissue bleaching¹⁶, fixed pancreases were dehydrated for 1hr at room temperature (RT) in increasing concentrations of methanol (50%, 80%, 100%) in 1X PBS. Then, the samples were incubated overnight at 4°C in a 6% hydrogen peroxide solution in 100% methanol, re-hydrated for 1hr at RT in increasing concentrations of methanol (100%, 100%, 80%, 50%) and finally washed for 1 hour in 1X PBS. Permeabilization and blocking were performed under rotation at 70 rpm at RT in PBSGT (1X PBS, 0.2% gelatin (Prolabo), and 0.5% Triton X-100 (Sigma-Aldrich)) as previously described²¹.

For whole-mount immunostaining, samples were incubated with the primary antibodies in a solution of PBSGT containing 0.1% saponin during 14 days at 37°C under rotation at 70 rpm. The primary antibodies employed were: goat anti-SOX9 (1:5,000, AF3075, R&D Systems), guinea pig anti-insulin (1:5,000, A0564, Dako), rabbit anti-SMA (1:1,000, ab5694, Abcam), mouse anti-CD34 (1:5,000, ab8536, Abcam), rabbit anti-TH (1:1,000, ab137869, Abcam), rabbit anti-PDX1⁸² (1:1,000), and mouse anti-NKX6.1 (1:1,000, F55A12, DSHB). Then, tissues were incubated with the secondary antibodies in a solution of PBSGT (0.1% saponin (10mg/mL)), during 4 days at 37°C under rotation

at 70 rpm. The secondary antibodies were: anti-guinea pig Alexa Fluor 488 (1:500, A-11073, Thermo Fisher Scientific), donkey anti-mouse Alexa Fluor 555 (1:500, ab150110, Abcam), donkey anti-rabbit 647 (1:500, ab150063, Abcam), donkey anti-rabbit 790 (1:250, ab186693, Abcam), and donkey anti-goat Alexa Fluor 790 (1:250, 705-655-147, Jackson Immuno). Next, samples were washed for 30 minutes in PBSGT at RT, embedded in 1.5% agarose (Roth) prepared in TAE 1X (Invitrogen)^{16,17} and stored at 4°C until tissue clearing.

In order to achieve tissue transparency, the samples were cleared using a modification from the iDISCO+ protocol²². Fetal pancreases were dehydrated in growing concentrations of methanol (20%, 40%, 60%, 80%, 100%, 100%, 1 hr each) at RT under rotation (14 rpm), next incubated overnight in a solution of 2/3 of DCM (dichloromethane) and 1/3 of methanol, next for 30 min in 100% DCM, and finally transferred to DBE (dibenzyl ether) for further storage and imaging.

3D imaging and processing

Acquisition was performed with Miltenyi Biotec Ultramicroscope Blaze (sCMOS camera 5.5MP) and Inspector Pro 7.3.2 acquisition software. Laser light sheets are generated at excitation wavelengths of 488, 561, 640, and 785nm. 4X magnification (MI Plan 4x NA0.35) and 12X magnification (MI Plan NA0.53) objective lenses were used. The Z step size between each image is 3 μ m. All the images were generated as tiff files, converted to Imaris files (.ims) by Imaris File Converter (v9.8, Bitplane), and visualized with Imaris (v9.8, Bitplane).

The 3D images, virtual slices, and movies were generated using Imaris x64 software (version 9.9.0, Bitplane). The acquired stack images were converted to imaris file images (.ims) using ImarisFileConverter software and the 3D images were reconstructed performed using the “volume rendering” function. To isolate a specific region of the tissue, the surface tool was used to manually segment. The 3D images, virtual slices and movies were generated using the “snapshot” and “animation” tools. To locate the pancreas in full intact PCW7 human embryo, the SOX9⁺ pancreatic area was delimited in consecutive slices.

Human and mouse pancreatic lengths and diameters were measured with the distance tool in virtual slices. The measurements of the SOX9⁺ and INS⁺ cluster volume and density were performed following the automatic segmentation tool. The distribution of human

INS⁺ clusters was measured in 3 virtual slices from 3 different pancreases. First, the pancreatic epithelium was manually outlined and the centroid (its center of mass) was determined for each slice. Then, the distance from every INS⁺ cluster was measured to the centroid. ⁸³.

Tissue culture

Human fetal pancreases were cultured for a maximum of 7 days at an air-complete medium interface in Petri dishes on 0.45µm filters (Millipore) as previously described (Attali et al., 2007; Huijbregts et al., 2019). Explants were cultured in G10 medium consisting of RPMI 1640 + glutaMax, 10% Fetal Bovine Serum (FBS), 1% Penicillin/Streptomycin, 1% HEPES and 1% non-essential amino-acids (61870036, ThermoFisher Scientific). Medium was replaced every 2 days. For EdU incorporation assays, pancreases were treated with 5 µM EdU for 4h, the reaction was stopped by washing out the tissue with G10 medium and immediate fixation. For experiments with PDGFAA, explants were cultured in DMEM/F12 medium (31331, ThermoFisher Scientific) containing ALK5i (10mM, 221234, Chem Cruz), noggin (500mg/mL, 120-10C, Peprotech) and nicotinamide (2.5M, 481907, Sigma). Explants were treated with PDGFAA (200ng/mL, PHG0035, Sigma) for 7 days, replacing the medium every 2 days.

References

1. Shih, H. P., Wang, A. & Sander, M. Pancreas organogenesis: from lineage determination to morphogenesis. *Annu. Rev. Cell Dev. Biol.* **29**, 81–105 (2013).
2. Atkinson, M. A., Campbell-Thompson, M., Kusmartseva, I. & Kaestner, K. H. Organisation of the human pancreas in health and in diabetes. *Diabetologia* **63**, 1966–1973 (2020).
3. Pan, F. C. & Wright, C. Pancreas organogenesis: from bud to plexus to gland. *Dev. Dyn.* **240**, 530–565 (2011).
4. Velazco-Cruz, L. *et al.* Acquisition of Dynamic Function in Human Stem Cell-Derived β Cells. *Stem Cell Reports* **12**, 351–365 (2019).
5. Pagliuca, F. W. *et al.* Generation of functional human pancreatic β cells in vitro. *Cell* **159**, 428–439 (2014).
6. Russ, H. A. *et al.* Controlled induction of human pancreatic progenitors produces functional beta-like cells in vitro. *EMBO J.* **34**, 1759–1772 (2015).
7. Gittes, G. K. Developmental biology of the pancreas: A comprehensive review. *Developmental Biology*. **326**, 4–35 (2009).
8. Oliver-Krasinski, J. M. & Stoffers, D. A. On the origin of the beta cell. *Genes Dev.* **22**, 1998–2021 (2008).
9. Larsen, H. L. & Grapin-Botton, A. The molecular and morphogenetic basis of pancreas organogenesis. *Semin. Cell Dev. Biol.* **66**, 51–68 (2017).
10. Jennings, R. E., Berry, A. A., Strutt, J. P., Gerrard, D. T. & Hanley, N. A. Human pancreas development. *Development (Cambridge)*. **142**, 3126–3137 (2015).
11. Jennings, R. E. *et al.* Development of the human pancreas from foregut to endocrine commitment. *Diabetes*. **62**, 3514–3522 (2013).
12. Villani, V. *et al.* SOX9+/PTF1A+ Cells Define the Tip Progenitor Cells of the Human Fetal Pancreas of the Second Trimester. *Stem Cells Transl. Med.* **8**, 1249–1264 (2019).
13. Jennings, R. E., Scharfmann, R. & Staels, W. Transcription factors that shape the

- mammalian pancreas. *Diabetologia*. **63**, 1974–1980 (2020).
14. Scharfmann, R. Control of early development of the pancreas in rodents and humans: implications of signals from the mesenchyme. *Diabetologia* **43**, 1083–1092 (2000).
 15. Nair, G. & Hebrok, M. Islet formation in mice and men: lessons for the generation of functional insulin-producing β -cells from human pluripotent stem cells. *Curr. Opin. Genet. Dev.* **32**, 171–180 (2015).
 16. Renier, N. *et al.* IDISCO: A simple, rapid method to immunolabel large tissue samples for volume imaging. *Cell*. **159**, 896–910 (2014).
 17. Belle, M. *et al.* A Simple Method for 3D Analysis of Immunolabeled Axonal Tracts in a Transparent Nervous System. *Cell Rep.* **9**, 1191–1201 (2014).
 18. Susaki, E. A. *et al.* Whole-brain imaging with single-cell resolution using chemical cocktails and computational analysis. *Cell*. **157**, 726–739 (2014).
 19. Chung, K. *et al.* Structural and molecular interrogation of intact biological systems. *Nat.* **497**, 332–337 (2013).
 20. de Medeiros, G., Balázs, B. & Hufnagel, L. Light-sheet imaging of mammalian development. *Semin. Cell Dev. Biol.* **55**, 148–155 (2016).
 21. Belle, M. *et al.* Tridimensional Visualization and Analysis of Early Human Development. *Cell*. **169**, 161–173 (2017).
 22. Renier, N. *et al.* Mapping of Brain Activity by Automated Volume Analysis of Immediate Early Genes. *Cell*. **165**, 1789–1802 (2016).
 23. McDonald, E. *et al.* SOX9 regulates endocrine cell differentiation during human fetal pancreas development. *Int. J. Biochem. Cell Biol.* **44**, 72–83 (2012).
 24. Slack, J. M. W. Developmental biology of the pancreas. *Development* **121**, 1569–1580 (1995).
 25. Jørgensen, M. C. *et al.* An illustrated review of early pancreas development in the mouse. *Endocr. Rev.* **28**, 685–705 (2007).
 26. Polak, M., Bouchareb-Banaei, L., Scharfmann, R. & Czernichow, P. Early pattern of differentiation in the human pancreas. *Diabetes*. **49**, 225–232 (2000).

27. Herrera, P. L. *et al.* Embryogenesis of the murine endocrine pancreas; early expression of pancreatic polypeptide gene. *Development*. **113**, 1257–1265 (1991).
28. Egozi, A. *et al.* Insulin is expressed by enteroendocrine cells during human fetal development. *Nat. Med.* **27**, 2104–2107 (2021).
29. Lammert, E., Cleaver, O. & Melton, D. Induction of pancreatic differentiation by signals from blood vessels. *Science*. **294**, 564–567 (2001).
30. Ramond, C. *et al.* Reconstructing human pancreatic differentiation by mapping specific cell populations during development. *Elife*. **6**:e27564 (2017).
31. Ramond, C. *et al.* Understanding human fetal pancreas development using subpopulation sorting, RNA sequencing and single-cell profiling. *Development* **145**: dev165480 (2018).
32. Scharfmann, R. *et al.* Development of a conditionally immortalized human pancreatic β cell line. *J. Clin. Invest.* **124**, 2087–2098 (2014).
33. Dixon, P. M. Ripley's K Function . *Encycl. Environmetrics* (2012) doi:10.1002/9780470057339.var046.pub2.
34. Miralles, F., Czernichow, P., Ozaki, K., Itoh, N. & Scharfmann, R. Signaling through fibroblast growth factor receptor 2b plays a key role in the development of the exocrine pancreas. *Proc. Natl. Acad. Sci. U. S. A.* **96**, 6267–6272 (1999).
35. Elghazi, L., Cras-Méneur, C., Czernichow, P. & Scharfmann, R. Role for FGFR2IIIb-mediated signals in controlling pancreatic endocrine progenitor cell proliferation. *Proc. Natl. Acad. Sci. U. S. A.* **99**, 3884–3889 (2002).
36. Balboa, D., Iworima, D. G. & Kieffer, T. J. Human Pluripotent Stem Cells to Model Islet Defects in Diabetes. *Front. Endocrinol. (Lausanne)*. **12**:642152 (2021).
37. Hogrebe, N. J., Maxwell, K. G., Augsornworawat, P. & Millman, J. R. Generation of insulin-producing pancreatic β cells from multiple human stem cell lines. *Nat. Protoc.* **16**, 4109–4143 (2021).
38. Mamidi, A. *et al.* Mechanosignalling via integrins directs fate decisions of pancreatic progenitors. *Nature*. **564**, 114–118 (2018).

39. Ameri, J. *et al.* Efficient Generation of Glucose-Responsive Beta Cells from Isolated GP2+ Human Pancreatic Progenitors. *Cell Rep.* **19**, 36–49 (2017).
40. Sever, D. & Grapin-Botton, A. Regeneration of the pancreas: proliferation and cellular conversion of surviving cells. *Curr. Opin. Genet. Dev.* **64**, 84–93 (2020).
41. Cozzitorto, C. *et al.* A Specialized Niche in the Pancreatic Microenvironment Promotes Endocrine Differentiation. *Dev. Cell.* **55**, 150-162 (2020).
42. Piper, K. *et al.* Beta cell differentiation during early human pancreas development. *J. Endocrinol.* **181**, 11–23 (2004).
43. Brissova, M. *et al.* Assessment of human pancreatic islet architecture and composition by laser scanning confocal microscopy. *J. Histochem. Cytochem.* **53**, 1087–1097 (2005).
44. Beydag-Tasöz, B. S. *et al.* Integrating single-cell imaging and RNA sequencing datasets links differentiation and morphogenetic dynamics of human pancreatic endocrine progenitors. *Dev. Cell* 14: S1534-5807(23)00366-0 (2023).
45. Cabrera, O. *et al.* The unique cytoarchitecture of human pancreatic islets has implications for islet cell function. *Proc. Natl. Acad. Sci. U. S. A.* **103**, 2334–2339 (2006).
46. Dai, C. *et al.* Islet-enriched gene expression and glucose-induced insulin secretion in human and mouse islets. *Diabetologia.* **55**, 707–718 (2012).
47. Scharfmann, R. *et al.* Mass production of functional human pancreatic β -cells: why and how? *Diabetes. Obes. Metab.* **18**, 128–136 (2016).
48. Cha, J. *et al.* Species-specific roles for the MAFA and MAFB transcription factors in regulating islet β cell identity. *JCI insight* **8**(16):e166386 (2023).
49. Ferrer, J., Benito, C. & Gomis, R. Pancreatic islet GLUT2 glucose transporter mRNA and protein expression in humans with and without NIDDM. *Diabetes.* **44**, 1369–1374 (1995).
50. De Vos, A. *et al.* Human and rat beta cells differ in glucose transporter but not in glucokinase gene expression. *J. Clin. Invest.* **96**(5):2489-95 (1995).
51. Henry, B. M. *et al.* Development of the human pancreas and its vasculature — An

- integrated review covering anatomical, embryological, histological, and molecular aspects. *Ann. Anat.* **221**, 115–124 (2019).
52. De Bakker, B. S. *et al.* An interactive three-dimensional digital atlas and quantitative database of human development. *Science* **354**(6315):aag0053 (2016).
 53. Glorieux, L. *et al.* Development of a 3D atlas of the embryonic pancreas for topological and quantitative analysis of heterologous cell interactions. *Development* **149**, (2022).
 54. Biemar, F. *et al.* Pancreas development in zebrafish: early dispersed appearance of endocrine hormone expressing cells and their convergence to form the definitive islet. *Dev. Biol.* **230**, 189–203 (2001).
 55. Hesselson, D., Anderson, R. M., Beinat, M. & Stainier, D. Y. R. Distinct populations of quiescent and proliferative pancreatic β -cells identified by HOCre mediated labeling. *Proc. Natl. Acad. Sci. U. S. A.* **106**, 14896–14901 (2009).
 56. Amat, F. & Keller, P. J. Towards comprehensive cell lineage reconstructions in complex organisms using light-sheet microscopy. *Dev. Growth Differ.* **55**, 563–578 (2013).
 57. Grüneboom, A. *et al.* Imaging innate immunity. *Immunol. Rev.* **306**, 293–303 (2022).
 58. Scharfmann, R., Xiao, X., Heimberg, H., Mallet, J. & Ravassard, P. Beta Cells within Single Human Islets Originate from Multiple Progenitors. *PLoS One* **3**:e3559 (2008).
 59. Deltour, L. *et al.* Polyclonal origin of pancreatic islets in aggregation mouse chimaeras. *Development.* **112**, 1115–1121 (1991).
 60. Scott Swenson, E. *et al.* Chimeric mice reveal clonal development of pancreatic acini, but not islets. *Biochem. Biophys. Res. Commun.* **379**, 526–531 (2009).
 61. Gouzi, M., Kim, Y. H., Katsumoto, K., Johansson, K. & Grapin-Botton, A. Neurogenin3 initiates stepwise delamination of differentiating endocrine cells during pancreas development. *Dev. Dyn.* **240**, 589–604 (2011).
 62. Sharon, N. *et al.* A Peninsular Structure Coordinates Asynchronous Differentiation

- with Morphogenesis to Generate Pancreatic Islets. *Cell*. **176**, 790-804 (2019).
63. Edsbagge, J. *et al.* Vascular function and sphingosine-1-phosphate regulate development of the dorsal pancreatic mesenchyme. *Development*. **132**, 1085–1092 (2005).
 64. Jacquemin, P. *et al.* An endothelial-mesenchymal relay pathway regulates early phases of pancreas development. *Dev. Biol.* **290**, 189–199 (2006).
 65. Ahrén, B. Autonomic regulation of islet hormone secretion--implications for health and disease. *Diabetologia* **43**, 393–410 (2000).
 66. Heinis, M. *et al.* Oxygen tension regulates pancreatic beta-cell differentiation through hypoxia-inducible factor 1alpha. *Diabetes* **59**, 662–669 (2010).
 67. Heinis, M. *et al.* HIF1 α and pancreatic β -cell development. *FASEB J.* **26**, 2734–2742 (2012).
 68. Golosow, N. & Grobstein, C. Epitheliomesenchymal interaction in pancreatic morphogenesis. *Dev. Biol.* **4**, 242–255 (1962).
 69. Attali, M. *et al.* Control of beta-cell differentiation by the pancreatic mesenchyme. *Diabetes* **56**, 1248–1258 (2007).
 70. Bhushan, A. *et al.* Fgf10 is essential for maintaining the proliferative capacity of epithelial progenitor cells during early pancreatic organogenesis. *Development* **128**, 5109–5117 (2001).
 71. Landsman, L. *et al.* Pancreatic mesenchyme regulates epithelial organogenesis throughout development. *PLoS Biol.* **9**: e1001143. (2011).
 72. Miralles, F., Czernichow, P. & Scharfmann, R. Follistatin regulates the relative proportions of endocrine versus exocrine tissue during pancreatic development. *Development*. **125**, 1017–1024 (1998).
 73. Capito, C. *et al.* Mouse muscle as an ectopic permissive site for human pancreatic development. *Diabetes*. **62**, 3479–3487 (2013).
 74. Gonçalves, C. A. *et al.* A 3D system to model human pancreas development and its reference single-cell transcriptome atlas identify signaling pathways required for progenitor expansion. *Nat. Commun.* **12**, 3144 (2021).

75. Sean, de la O. *et al.* Single-Cell Multi-Omic Roadmap of Human Fetal Pancreatic Development. *bioRxiv* (2022) doi:10.1101/2022.02.17.480942.
76. Ma, Z. *et al.* Deciphering early human pancreas development at the single-cell level. *Nat. Commun.* **14**, 5354 (2023).
77. Castaing, M. *et al.* Blood glucose normalization upon transplantation of human embryonic pancreas into beta-cell-deficient SCID mice. *Diabetologia.* **44**, 2066–2076 (2001).
78. Evtouchenko, L., Studer, L., Spencer, C., Dreher, E. & Seiler, R. W. A mathematical model for the estimation of human embryonic and fetal age. *Cell Transplant.* **5**, 453–464 (1996).
79. Huijbregts, L. *et al.* Bromodomain and extra terminal protein inhibitors promote pancreatic endocrine cell fate. *Diabetes.* **68**, 761–773 (2019).
80. Huijbregts, L. *et al.* Culture, differentiation, and transduction of mouse E12.5 pancreatic spheres: an in vitro model for the secondary transition of pancreas development. *Islets.* **13**, 10–23 (2021).
81. Castaing, M., Duvillié, B., Quemeneur, E., Basmaciogullari, A. & Scharfmann, R. Ex vivo analysis of acinar and endocrine cell development in the human embryonic pancreas. *Dev. Dyn.* **234**, 339–345 (2005).
82. Duvillié, B., Attali, M., Aiello, V., Quemeneur, E. & Scharfmann, R. Label-retaining cells in the rat pancreas: Location and differentiation potential in vitro. *Diabetes.* **52**, 2035–2042 (2003).
83. Schindelin, J. *et al.* Fiji: an open-source platform for biological-image analysis. *Nat. Methods.* **9**, 676–682 (2012).
84. Baddeley, A., Rubak, E. & Turner, R. Spatial Point Patterns. *Spat. Point Patterns* (2015).

Acknowledgements

This project has received funding from the European Union's Horizon 2020 research and innovation program under grant agreement no. 874839 (RS, HS), INSERM cross-cutting program HuDeCA 2018, Fondation pour la Recherche Medicale EQU201903007793, the Fondation Bettencourt Schueller (RS) and the Fondation Francophone pour la Recherche sur le Diabete (FFRD) (RS). The RS laboratory belongs to the Laboratoire d'Excellence consortium Revive (Investissements d'Avenir ANR-10-LABX-73-01).

Author contributions

A.V, Y.G, M.I, and R.B performed tissue clearing, immunostaining, imaging, data visualization and analysis. A.V, V.A, and L.R performed tissue processing and culture. M.T and S.M-G collected the human embryo samples. A.V, Y.G, A.C, and R.S wrote the manuscript. HS provided some of the protocols. All authors contributed to the discussion and interpretation of the results.

Competing interests

The authors declare no conflict of interests.

Figure legends

Fig 1. Human embryonic and fetal pancreases display isometric growth from PCW5 to 11.

LSFM images of embryonic and fetal pancreases (a-e) immunostained for SOX9 or SOX9 and TH (a, a', b). **a-a'** Frontal and lateral 3D views of a PCW7 human embryo revealing the anatomical location of the human pancreas (magenta). SOX9 is expressed in the cartilage and various organs including the pancreas. **b** Sagittal section of a PCW7 human embryo locating the pancreas and adjacent tissues. **c, d** At PCW5.7, SOX9 staining labels both ventral and dorsal buds, that have fused at PCW6.4. **e** Tridimensional SOX9 immunostaining (white) in whole mount pancreases dissected from human embryos and fetuses between PCW5 and 11. Dashed red line depicts the diameter of the organ. **f** Determination of the length, **g** the diameter, and **h** the diameter to length ratio of the pancreases from PCW PCW5-11.

Scale bar: 2mm (a, a'), 500 μ m (b, e), 200 μ m, (c and d).

Abbreviations: R, right; L, left; V, ventral; D, dorsal; Panc, pancreas.

Fig 2. Spatial and time determination of INS⁺ cell location in the pancreatic primordium.

LSFM images of embryonic and fetal pancreases (a-e, i, j) immunostained for SOX9 (green) and insulin (white). **a** At PCW5.7, a few clusters of insulin-immunoreactive (INS⁺) cells are found at the center of the dorsal bud (Db). **b** Representative image of extra-pancreatic INS⁺ cells that were detected in a gut region adjacent to the head of the pancreas (PCW 7.4) (n=4 pancreases). **c-d** Magnification of panel B, showing the gut region next to the pancreas containing INS⁺ clusters. The dashed line depicts the region of the 2D section shown in the panel (E). **e** Section showing the location of INS⁺ clusters (white) within the gut region next to the pancreas (SOX9 outlined in green). **f** Determination of the number of INS⁺ clusters from PCW5-11. **g** Determination of INS⁺ cluster density (volume of INS⁺ clusters / volume SOX9⁺ epithelium) from PCW5-11. **h** Quantification of the number of INS⁺ cell per cluster at PCW6, full sectioned and stained

to include all the INS⁺ clusters (n=3). **i** At PCW9, INS⁺ clusters are aligned to the center of the pancreas as shown in 3D. The dashed line represents a sagittal section. **j** Transversal view of panel **i**. **k** Histogram showing the distribution of the INS⁺ clusters across the pancreatic epithelium in 2D sections from three PCW8 specimens (Sample A, B, and C). The x axis represents the distance of the INS⁺ clusters to the center of the pancreas.

Scale bar: 250µm (a), 300µm (b), 150 µm (c and d), and 200µm (e, i and j).

Abbreviations: Db: Dorsal bud; Vb: Ventral bud; R, right; L, left; V, ventral; D, dorsal; Panc, pancreas.

Fig 3. 3D analysis of pancreatic growth and beta cell development in mice. a-c Growth of the mouse fetal pancreas from E10 to E16. SOX9 in green and INS in white (n=4). White arrow depicts the pancreatic primordium. **d-g** Length (right-left axis), diameter (ventral-dorsal axis), diameter to length ratio measurements and INS⁺ clusters number in 3D images of murine fetal pancreases at E10, E12 and E16. *P value < 0.05, Mann-Whitney test (n=4). **h** Table matching the developmental stages of mouse and human embryonic and fetal pancreases.

Scale bar: 500µm (a-c).

Abbreviations: R, right; L, left; V, ventral; D, dorsal; T: Top; B: Bottom.

Fig 4. Proliferation of human embryonic and fetal pancreatic cells. a-b Representative staining for PDX1 (green) and KI67 (red) on sections of human fetal pancreas at PCW9 and quantification of the frequency of PDX1⁺/KI67⁺ at PCW7, 9 and 11 (n=3). **c-d** Representative staining for INS (green) and KI67 (red) on sections of human fetal pancreas at PCW9 and quantification of the frequency of INS⁺/KI67⁺ at PCW7, 9 and 11. Inset reveals a single INS⁺KI67⁺ cell. **e** Heatmap showing the expression of cell cycle-related genes in 3 successive populations of pancreatic progenitors: ECAD⁺CD142⁺(pink); ECAD⁺CD142⁻(green); ECAD^{low}CD142⁻SUSD2⁺ (blue). **f** Proliferating pancreatic progenitors (PDX1⁺/EdU⁺) across the pancreatic epithelium.

PDX1 in green, EdU in red and E-CADH in white (n=6). **g** Computation of the Ripley K function ($K(r)$) to determine the distribution pattern of PDX1⁺KI67⁺ progenitors in 2D images at PCW7, 9 and 11. Red lines represent the random distribution while each black line represent the quantification of the Ripley K Function ($K(r)$) for PDX1⁺KI67⁺ progenitors in a single 2D image. **h** Expected output of the Ripley K function ($K(r)$) computed for three different types of spatial distribution: random, aggregate and regular. **i** Determination of the cell identity of peripheral pancreatic cells. CPA1 in green and KI67 in red in a human fetal pancreas at PCW11.

Scale bar: 100 μ m (a and c), 500 μ m (f), 1 mm (i).

Fig 5. Effect of PDGFAA in explants of human embryonic and fetal pancreases. **a** Heatmap showing the expression of PDGFRA and PDGFRB in the mesenchymal and epithelial fraction of human fetal pancreases. Epithelial (EPCAM) and mesenchymal markers (CD248) are used as positive controls for each population. **b-c** Expression pattern of PDGFRA and PDGFRB (green) in a human fetal pancreas at PCW10, ECADH is in red. **d** Macroscopic integrity of the tissue at day 7 in control or treated samples. **e** Determination of the proliferation ratio for pancreatic progenitors at day 7 treated or not with PDGFAA (n=6). Mean \pm SD. **f-g** Representative images of control and treated (PDGFAA) samples at day 7 stained with PDX1 (green) and KI67 (red).

Scale bar: 150 μ m (b, c, g and f), 1mm (d).

Movie 1, related to Supplementary Figure 1. Expression pattern of SOX9, PDX1 and NKX6.1 in the human fetal pancreatic epithelium. Staining of SOX9 (cyan), PDX1 (magenta) and NKX6.1 (yellow) in the human pancreatic epithelium at PCW8.

Movie 2, related to Figure 1. Anatomical location of the pancreas in the human embryo. Human specimen at PCW7 stained with SOX9 and TH in white. The pancreas is highlighted in magenta.

Movie 3, related to Figure 1. Detection of ventral and dorsal buds with light-sheet fluorescence microscopy in human embryonic pancreas at PCW5.7. SOX9 in white.

Movie 4, related to Figure 2. Temporal location of the first INS⁺ cells in the human embryonic pancreas. Pancreas at PCW5.7 stained with SOX9 in green and INS in white.

Movie 5, related to Figure 2. Detection of extra-pancreatic INS⁺ cells in the human embryonic gut with light-sheet fluorescence microscopy. Pancreas at PCW7.4 stained with SOX9 in green and INS in white.

Movie 6, related to Figure 2. Spatial location of INS⁺ clusters in the human fetal pancreas. Pancreas at PCW8 stained with SOX9 in green and INS in white.

Tables

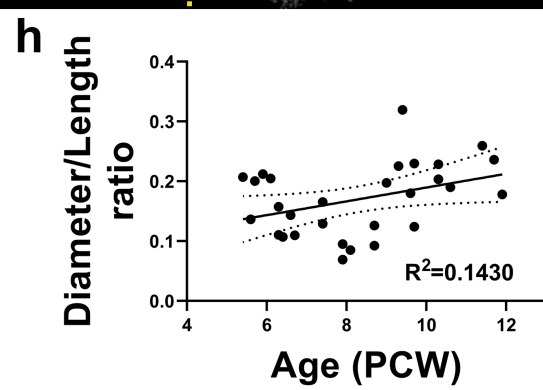
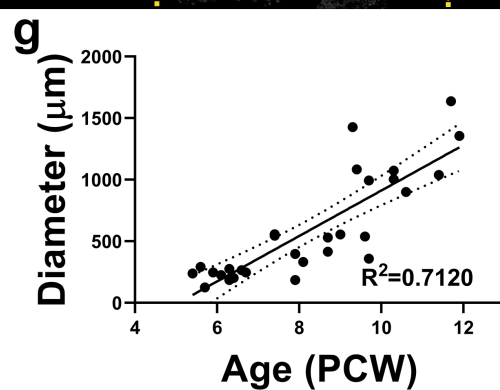
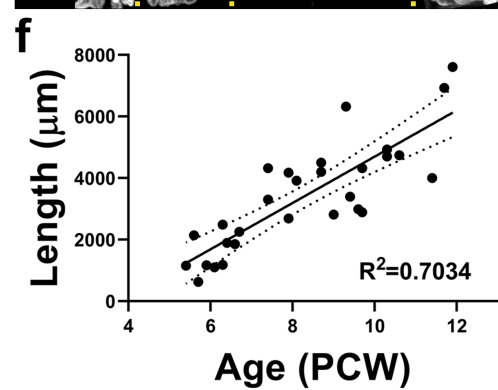
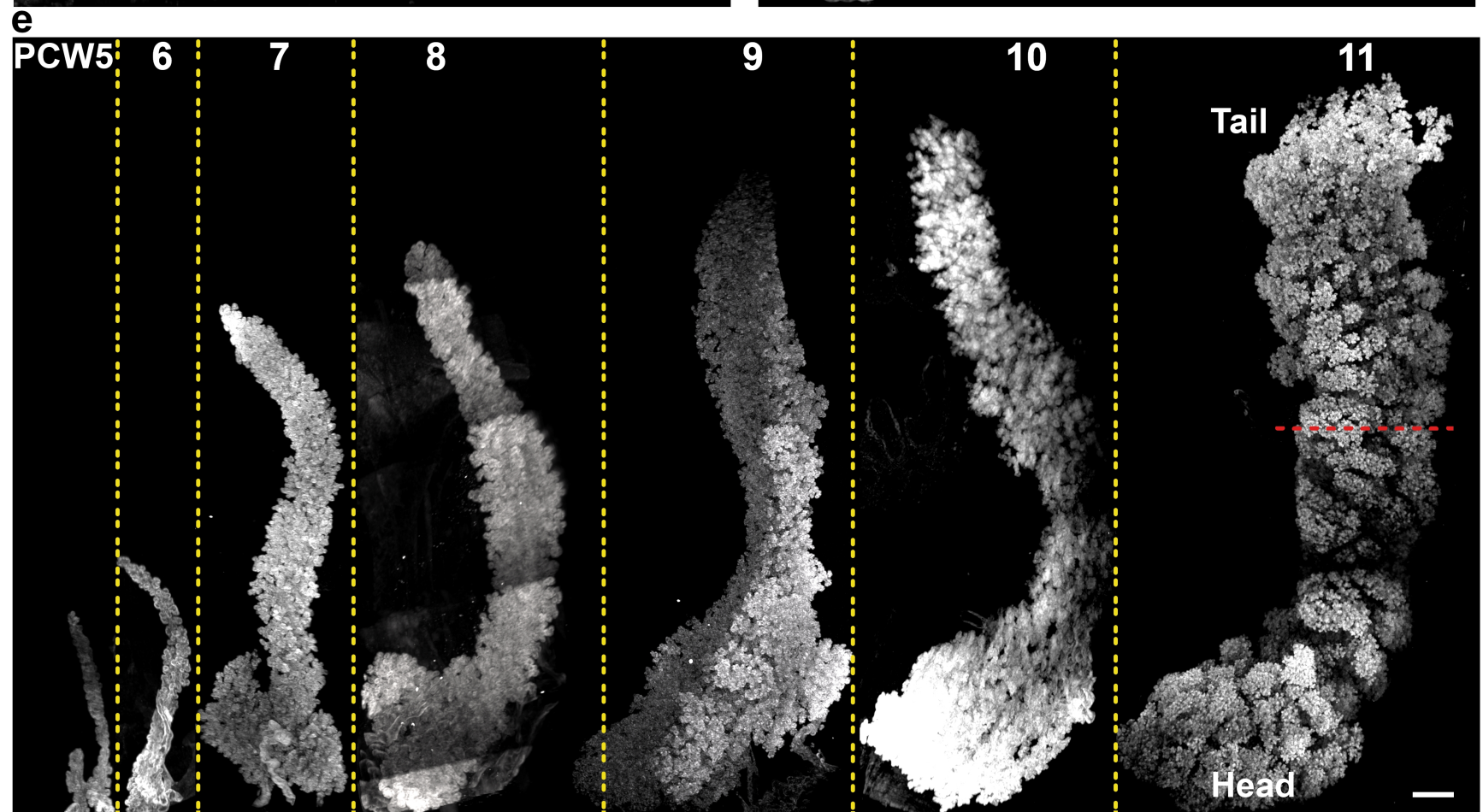
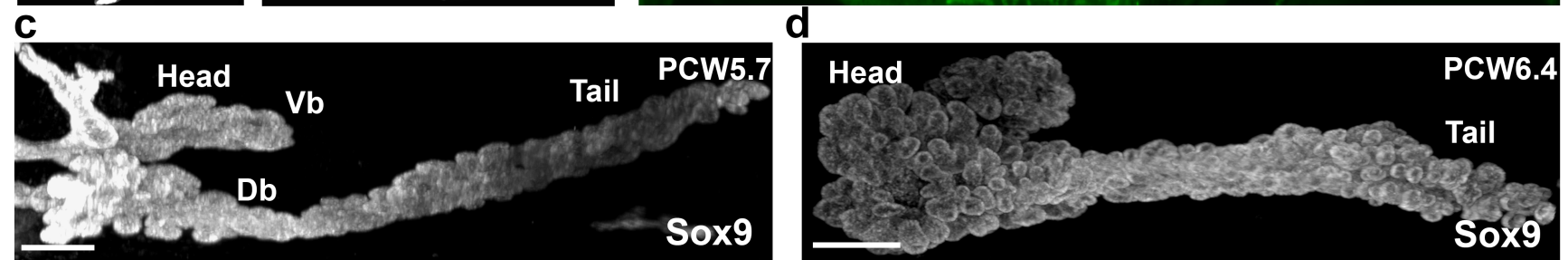
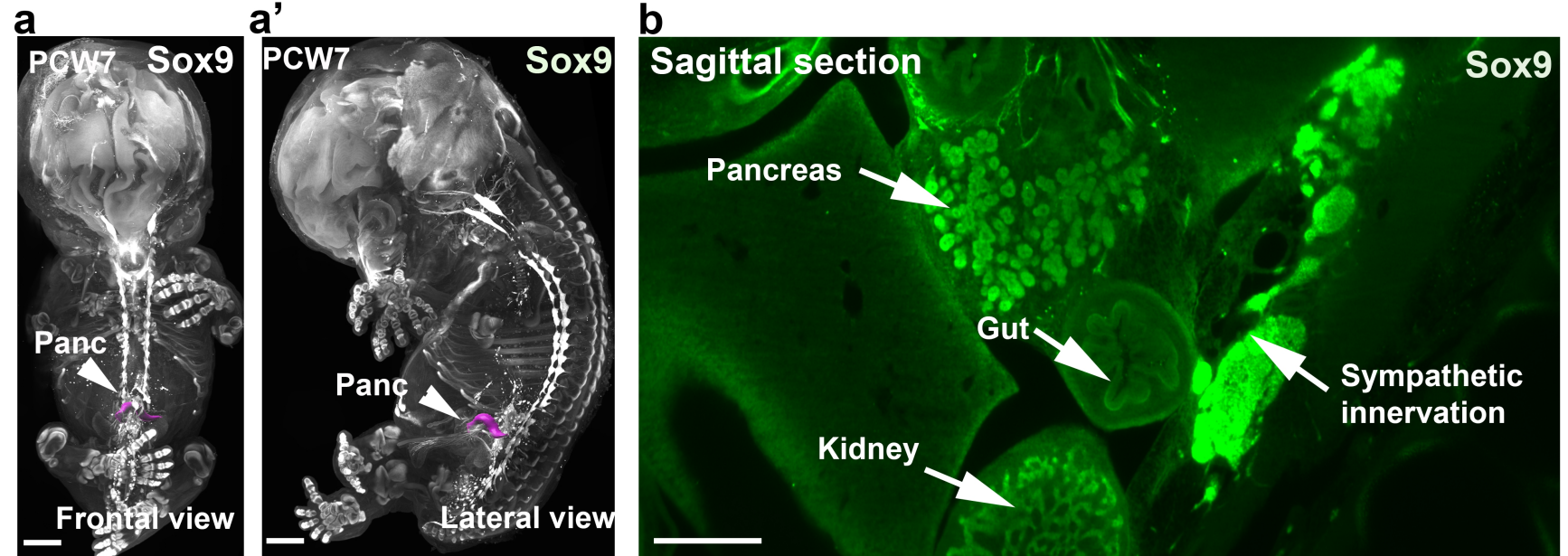
Table 1. Human embryonic and fetal pancreases grouped by age employed in 3D immunostainings. A total of 29 human fetal tissues from PCW5-11 were used for the experiments of 3D immunostaining, with a minimum of 3 samples per age.

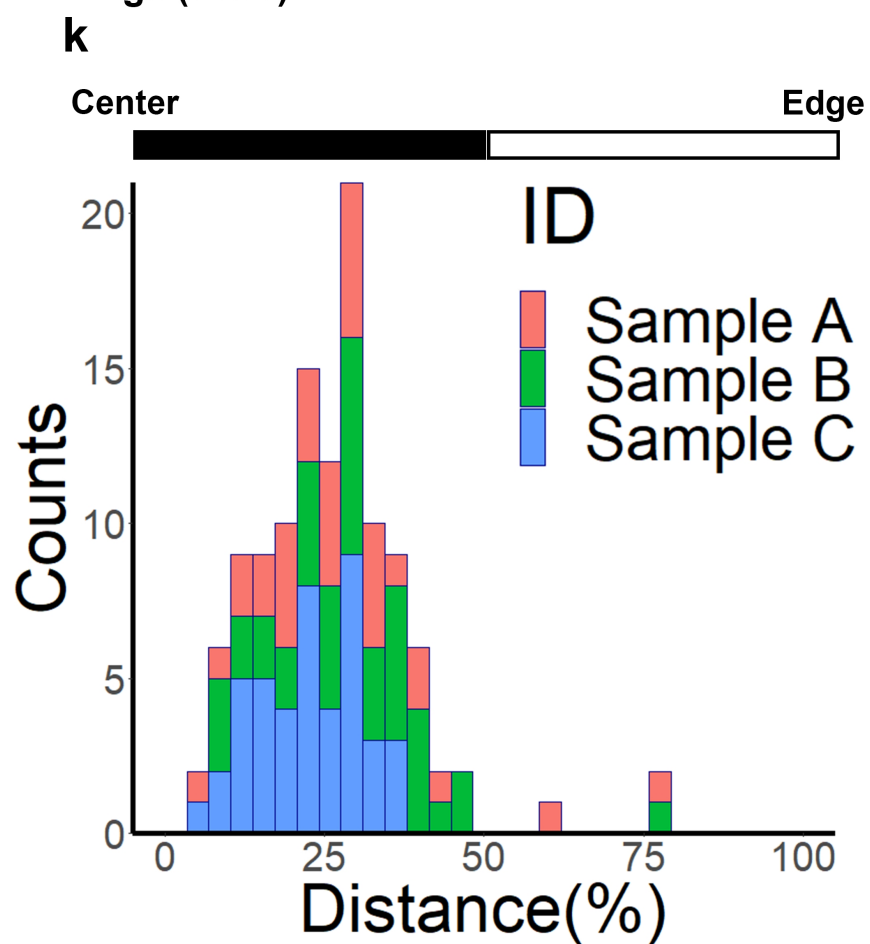
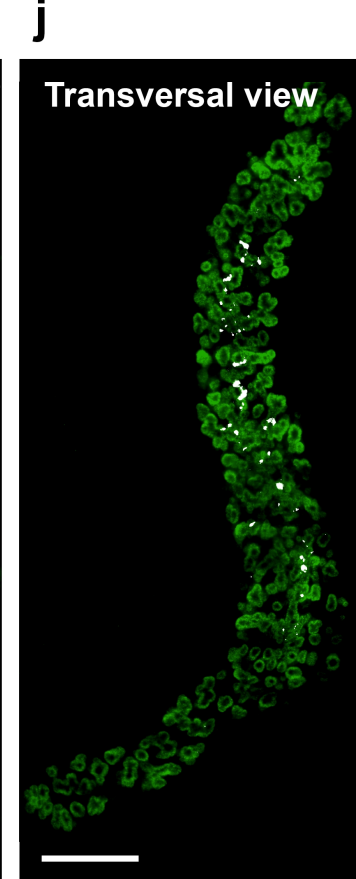
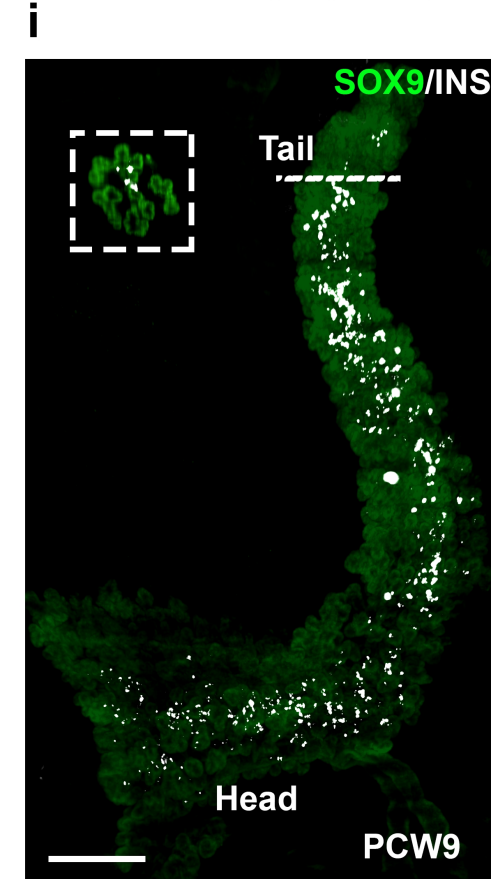
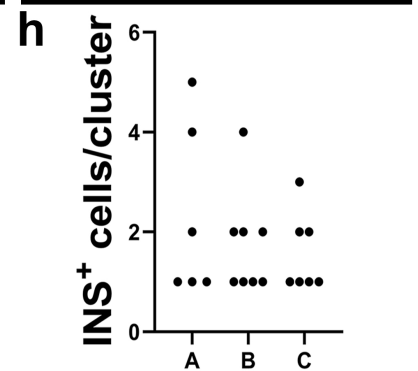
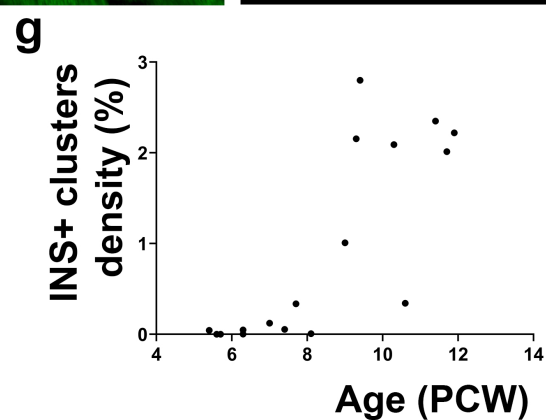
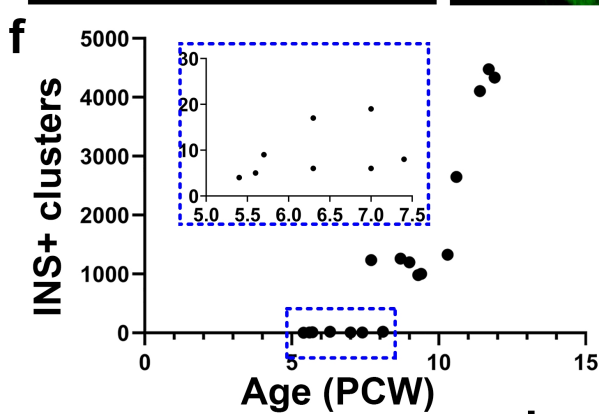
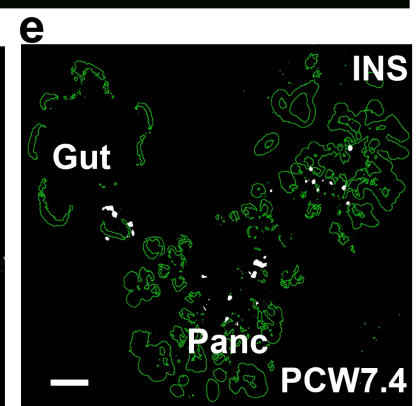
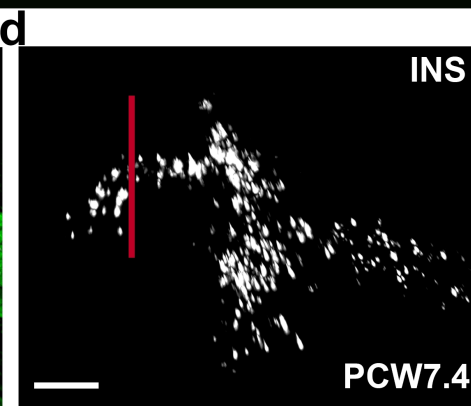
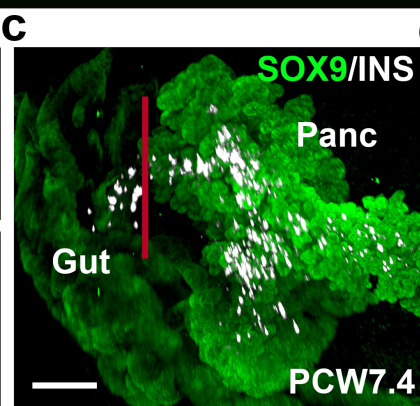
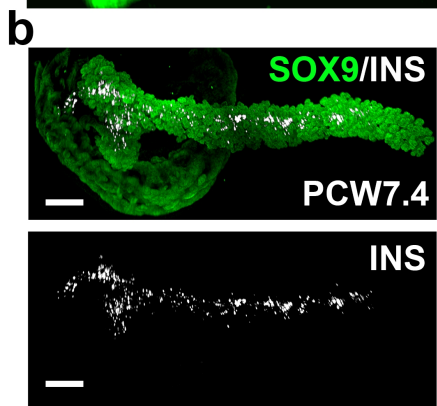
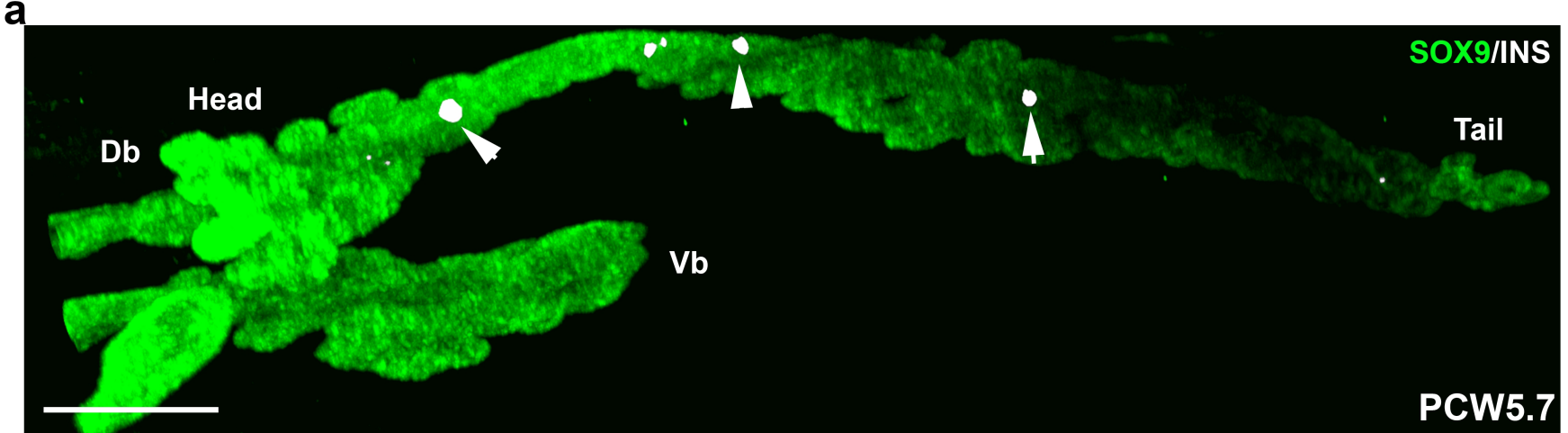
AGE (PCW)	SAMPLE SIZE
5 – 5.9	4
6 – 6.9	6
7 – 7.9	4
8 – 8.9	3
9 – 9.9	6
10 – 10.9	3
11 – 11.9	3
<u>TOTAL</u>	<u>29</u>

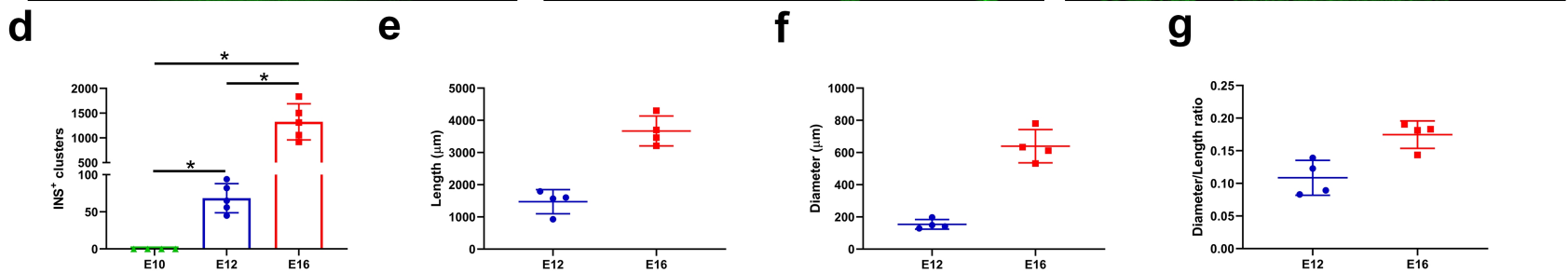
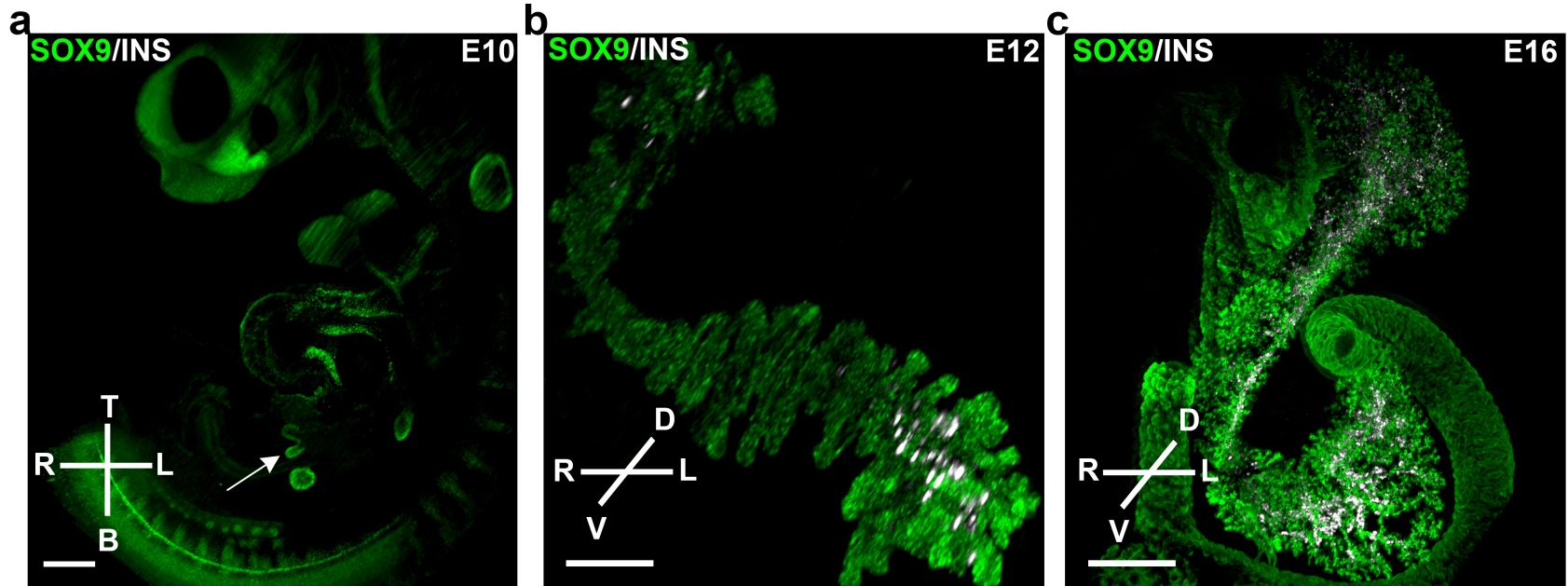
Table 2. Human embryonic and fetal pancreases represented in each figure and panel. Each specimen appearing in all the figures is labeled and records the sex information.

Figure	Panel	Specimen Number	Sex	Staining
1	A-B	Ac713	Male	SOX9/TH
1	C	EH3912	Male	SOX9
1	D	EH3333	Male	SOX9
1	E	EH3912 (PCW5)	Male	SOX9
1	E	EH3374 (PCW6)	Male	SOX9
1	E	EH3674 (PCW7)	Male	SOX9
1	E	EH3079 (PCW8)	Male	SOX9
1	E	EH3984 (PCW9)	Female	SOX9
1	E	EH3950 (PCW10)	Male	SOX9
1	E	EH3084 (PCW11)	Male	SOX9
2	A	EH3912	Male	SOX9/INS
2	B-E	EH3363	Female	SOX9/INS
2	I-J	EH4201	Male	SOX9/INS
4	A	EH3522	Female	PDX1/KI67
4	C	EH3522	Female	PDX1/INS
4	F	EH4150	Female	PDX1/ECADH/EDU
4	I	EH4015	Female	CPA1/KI67
5	B-C	EH3630	Female	PDGFRA/PDGFRB/ECADH

5	F	EH4342	Male	PDX1/KI67
5	G	EH4360	Female	PDX1/KI67
Supp. 1	A	EH4091	Male	SOX9/PDX1/NKX6.1
Supp. 1	B	EH3524	Male	SOX9/PDX1/NKX6.1
Supp. 2	A	EH3155	Male	SOX/INS/CD34
Supp. 2	B	EH3877	Male	SOX/INS/SMA
Supp. 3	A	EH4255	Female	PDX1/KI67
Supp. 3	B	EH4300	Male	PDX1/NKX6.1
Movie 1		EH4089	Female	SOX9/PDX1/NKX6.1
Movie 2		AC713	Male	SOX9/TH
Movie 3		EH3912	Male	SOX9
Movie 4		EH3912	Male	SOX/INS
Movie 5		EH3363	Female	SOX/INS
Movie 6		EH3674	Male	SOX/INS







h

	Murine	E10	E12	E16
DIFFERENTIATION		-	+	+++
	Human	5 PCW	8 PCW	11 PCW
		-	+	+++

